

# Judd–Ofelt Intensity Parameters and Spectral Properties of Gd<sub>2</sub>O<sub>3</sub>:Eu<sup>3+</sup> Nanocrystals

Chunxu Liu\* and Junye Liu

Key Laboratory of Excited States Processes, Changchun Institute of Optics, Fine Mechanics and Physics, Chinese Academy of Sciences, Changchun, 130033, China

Kai Dou

College of Medicine, University of Kentucky, Lexington, Kentucky 40536

Received: May 19, 2006; In Final Form: July 30, 2006

Three nonequivalent centers of  $C_3$  (A, B, and C) in monoclinic phase and  $C_2$  and  $S_6$  centers in cubic phase were identified in the Gd<sub>2</sub>O<sub>3</sub>:Eu<sup>3+</sup> nanocrystals with spectral techniques. Size dependence in the spectra indicated that the excitations from both host and charge-transfer band (CTB) for the  $^5D_0 \rightarrow ^7F_2$  transition of Eu<sup>3+</sup> ions were nearly equal for a larger size of 135 nm of the cubic phase; however, with decreasing the size to or less than 23 nm, the excitations by the CTB dominated. The variation of excitation leading to the symmetry and energy change in the  $C_2$  and  $S_6$  sites was also observed for larger particle sizes. The Judd–Ofelt intensity parameters  $\Omega_\lambda$  ( $\lambda = 2, 4$ ) for Gd<sub>2</sub>O<sub>3</sub>:Eu<sup>3+</sup> nanoparticles were experimentally determined. The parameters  $\Omega_\lambda$  were found to significantly change with the sizes of Gd<sub>2</sub>O<sub>3</sub>:Eu<sup>3+</sup> from nanoparticles to bulk material. With decreasing the size from 135 to 15 nm, the quantum efficiencies for  $^5D_0$  reduced from 23.6% to 4.6% due to the increasing ratio of surface to volume.

## 1. Introduction

Rare earth sesquioxide is one of the typical phosphor materials for hosting trivalent ions. Three structures were found in the sesquioxides, known as hexagonal, cubic, and monoclinic phases. The lattice distortion in Gd<sub>2</sub>O<sub>3</sub>:Eu<sup>3+</sup> from doped Eu<sup>3+</sup> ions is insignificant due to nearly identical radii of 0.094 for Gd<sup>3+</sup> ion and 0.095 nm for Eu<sup>3+</sup>. The structure transition of Gd<sub>2</sub>O<sub>3</sub> from cubic to monoclinic phase occurs at  $\geq 1250$  °C. The Eu<sup>3+</sup> ions substitute the Gd<sup>3+</sup> ions in Gd<sub>2</sub>O<sub>3</sub>:Eu<sup>3+</sup> and occupy the lattice sites  $C_2$  and  $S_6$  in the cubic phase and three nonequivalent sites (A, B, and C) in the monoclinic phase, respectively.<sup>1</sup>

Eu<sup>3+</sup>-doped Gd<sub>2</sub>O<sub>3</sub> nanocrystallines have shown very rich luminescent features due to the possible paths of activating the trivalent rare-earth ion Eu<sup>3+</sup> through different sensitization processes, e.g., the host Gd<sub>2</sub>O<sub>3</sub> absorption, Eu–O charge transfer, the Gd<sup>3+</sup> ion absorption, and the Eu<sup>3+</sup> ion self-excitation. The initial state possesses, usually, the same parity as the final one. However, the  $4f^n$ -transitions leading to luminescence were experimentally observed for Eu<sup>3+</sup> ions in Gd<sub>2</sub>O<sub>3</sub>:Eu<sup>3+</sup> nanocrystallines. The mixture of opposite-parity state configurations, for example, the  $4f^{n-1}5d$  and charge transfer states, may make these transitions partially allowed. It is well-known that the excitations from the host band and charge-transfer band (CTB) for the  $^5D_0 \rightarrow ^7F_2$  transition of Eu<sup>3+</sup> ions are almost equal for the bulk Gd<sub>2</sub>O<sub>3</sub>. The Eu<sup>3+</sup> ions were excited by the  $4f^n$  energy levels in most previous investigations, rarely by CTB. In the current paper, the size impact on the excitation processes from  $C_2$  and  $S_6$  sites has been investigated in Gd<sub>2</sub>O<sub>3</sub>:Eu<sup>3+</sup> nanocrystalline having different particle sizes.

The spectral properties of Gd<sub>2</sub>O<sub>3</sub>:Eu<sup>3+</sup> nanoparticles at 77 K were investigated using Judd–Ofelt theory.<sup>2,3</sup> Intensity param-

eters  $\Omega_\lambda$  ( $\lambda = 2, 4$ ) were calculated by using the experimental data associated with the  $^5D_0 \rightarrow ^7F_2$  and  $^5D_0 \rightarrow ^7F_4$  transitions by comparing the magnetic dipole transition of  $^5D_0 \rightarrow ^7F_1$  as reference.<sup>4</sup> Our results indicated that intensity parameters of  $\Omega_\lambda$  varied with nanoparticle sizes of Gd<sub>2</sub>O<sub>3</sub>:Eu<sup>3+</sup> and significant differences were found in these parameters between nanoparticles and bulk materials. With decreasing the particle sizes from 135 to 15 nm, the quantum efficiency for the  $^5D_0$  band in Gd<sub>2</sub>O<sub>3</sub>:Eu<sup>3+</sup> nanoparticles reducing from 23.6% to 4.6% was observed. A possible enhancement of the nonradiation relaxation rate from the large ratios of surface to volume would be the reason to decrease the luminescent quantum efficiencies of nanoparticles. The impact of the charge transfer state of (Eu<sup>3+</sup>–O<sup>2-</sup>) and multiphonon nonradiative re-excitation on spectral properties was also studied in this paper.

## 2. Site-Selective Excitation and Energy Transfer

**2.1. X-ray Diffraction (XRD) Patterns.** The nanocrystal samples were prepared by using combustion synthesis.<sup>5</sup> The samples were annealed at several temperatures to obtain different particle sizes. Sample 1 is Gd<sub>1.9</sub>Eu<sub>0.1</sub>O<sub>3</sub> annealed at 600 °C for 1 h, sample 2 is Gd<sub>1.8</sub>Eu<sub>0.2</sub>O<sub>3</sub> annealed at 1000 °C for 1 h, and sample 3 is Gd<sub>1.8</sub>Eu<sub>0.2</sub>O<sub>3</sub> annealed at 800 °C for 1 h.

XRD analyses were carried out on a Shimadzu XD-3A powder X-ray diffractometer with Cu K $\alpha$  radiation at  $\lambda = 1.5418$  Å. The XRD patterns of the three samples 1, 2, and 3 are shown in Figure 1. The particle sizes of the nanoparticles were determined by using the Scherrer formula  $D = k\lambda/B \cos \theta$  and transmission electron microscope (TEM). The XRD pattern of sample 1 was wider than that of sample 2. The size and structure were therefore determined to be 10 nm in diameter for sample 1 and bulk material for sample 2 with the same monoclinic phases for both samples and 30 nm for sample 3 having the cubic phase.

\* Address correspondence to this author. Fax: +86-431-6176337. E-mail: cxliu@ciomp.ac.cn.

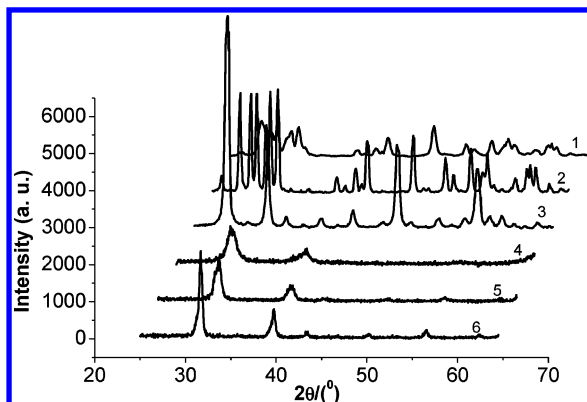


**Figure 1.** 1. XRD spectra of  $\text{Gd}_2\text{O}_3:\text{Eu}^{3+}$ : (1) monoclinic nanomaterial (10 nm); (2) monoclinic bulk material; (3) cubic nanomaterial (30 nm); (4) sample 4 (15 nm); (5) sample 5 (23 nm); and (6) sample 6 (135 nm), respectively.

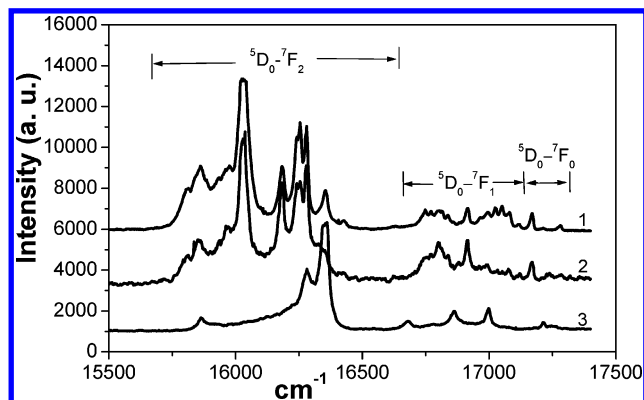


**Figure 2.** 2. PL spectra of  $\text{Gd}_2\text{O}_3:\text{Eu}^{3+}$  for  ${}^5\text{D}_0 \rightarrow {}^7\text{F}_{0,1,2}$  exciting at 355 nm: (1) monoclinic nanoparticles (10 nm) at 10 K; (2) monoclinic bulk material at 77 K; and (3) cubic nanoparticles (30 nm) at 77 K.

**2.2. PL and Site-Selective Spectra.** PL measurements of  $\text{Gd}_2\text{O}_3:\text{Eu}^{3+}$  were performed by using the third harmonic of a YAG:Nd laser at 355 nm. Site-selective excitation (SSE) spectra were measured with a dye laser (filled with Rh6G tunable from 570 to 610 nm) pumped by the second harmonic of a YAG:Nd laser. The spectrum was recorded by the Spex-1403 monochromator with double gratings. A boxcar integrator provided electronically gated signal processing.

The electronic configuration of rare earth Eu is  $(4f^7, 6s^2)$ . The outer layer electronic configuration of trivalent  $\text{Eu}^{3+}$  is  $4f^6$ . The intraconfigurational dipole transition is thus strictly forbidden by the parity selection rule. However, the parity selection rule is broken while the crystallines lack an inversion center, and the forbidden transitions become partially allowed. Figure 2(1–3) shows the emission spectra for the  ${}^5\text{D}_0 \rightarrow {}^7\text{F}_J$  ( $J = 0, 1, 2$ ) transitions for three  $\text{Gd}_2\text{O}_3:\text{Eu}^{3+}$  samples under 355 nm excitation at 10 and 77 K, respectively. In Figure 2(1), three spectral peaks located at 17 292, 17 224, and 17 179  $\text{cm}^{-1}$  were observed, and assigned to the  $\text{Eu}^{3+}$  ions occupying the monoclinic crystallographic sites. An examination of these figures reveals that the luminescent spectra of the monoclinic nanocrystallines show the same spectral distribution as bulk material in the PL spectra (Figures 2(1) and 2(2)) and, however, different spectral structures from that of the cubic phase as shown in Figure 2(3).

There are at least three kinds of luminescent centers according to three spectral peaks observed in PLE (Figure 3a–h) for monoclinic nanomaterial having a particle size of 10 nm. Comparing with ref 1, three different emission centers denoted as A, B, and C with  $C_s$  symmetry can be identified. Curve i in

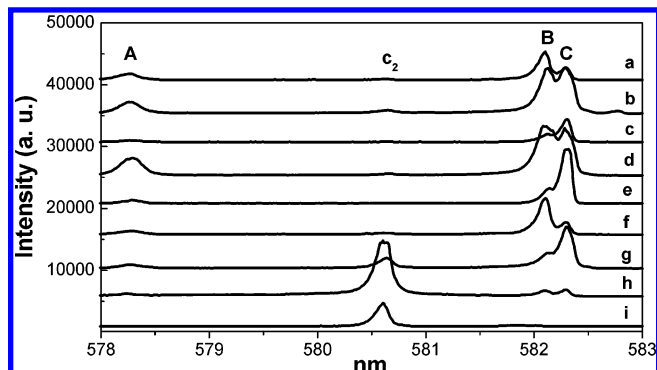


**Figure 3.** 3. (a–h) PLE spectra of monoclinic nano- $\text{Gd}_2\text{O}_3:\text{Eu}^{3+}$  at 10 K, monitoring positions at (a) 15 854, (b) 16 013, (c) 16 032, (d) 16 047, (e) 16 190, (f) 16 242, (g) 16 279, and (h) 16 361  $\text{cm}^{-1}$ . (i) PLE spectra of cubic nano- $\text{Gd}_2\text{O}_3:\text{Eu}^{3+}$  at 77 K, monitoring the position at 16 361  $\text{cm}^{-1}$ .

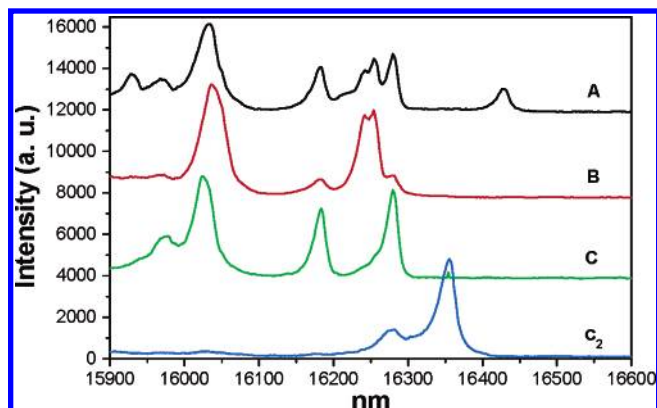


**Figure 4.** 4. Site-selective excitation spectra of nano- $\text{Gd}_2\text{O}_3:\text{Eu}^{3+}$  at 10 K, with exciting wavelengths at (A) 578.3 (17 292  $\text{cm}^{-1}$ ), (B) 582.1 (17 191  $\text{cm}^{-1}$ ), (C) 582.3 (17 173  $\text{cm}^{-1}$ ), and (c<sub>2</sub>) 580.6 nm (17 224  $\text{cm}^{-1}$ ).

Figure 3 comes from  $C_2$  sites of cubic structure according to the peak at 580.6 nm (17 223  $\text{cm}^{-1}$ ) in the PLE spectrum of the cubic nanocrystal (sample 3 ( $\text{Gd}_{1.8}\text{Eu}_{0.2}\text{O}_3$ )) at a monitoring wavenumber of 16 361  $\text{cm}^{-1}$  (611.2 nm). Sample 1 has the excitations from the  $C_2$  sites of cubic structure in the monoclinic phase indicating the existence of the mixing of monoclinic and cubic phases. This is consistent with the result from the XRD.

The site-selective excitation spectra are shown in Figure 4. The different emission spectral distribution can be attributed to  $C_s$  and  $C_2$  selectively excited. When the center A is excited, the strong emissions from B and C centers can be observed, indicating that the energy is effectively transferred from the center A to centers of B and C.

### 3. Photoluminescence Properties and J–O Parameters in nano- $\text{Gd}_2\text{O}_3:\text{Eu}^{3+}$

**3.1. Charge-Transfer Excitation of  $\text{Eu}^{3+}$  with  $C_2$ ,  $S_6$  Sites in the Nanocrystal  $\text{Gd}_2\text{O}_3:\text{Eu}^{3+}$ .** The emissions from  $4f^6$  electronic states of  $\text{Eu}^{3+}$  ion have been intensively studied in the past decades, but to our knowledge, only a limited number of publications discussed the luminescence of nanosized materials doped with  $\text{Eu}^{3+}$  ions excited by the charge-transfer process.<sup>6–8</sup> Charge-transfer excited  $\text{Gd}_2\text{O}_3:\text{Eu}^{3+}$  comprises the electronic distribution changes of the Eu–O couple. Effective optical emissions would be remarkably enhanced when the charge-transfer state through nonradiative relaxation to the  ${}^5\text{D}_0$  in  $\text{Eu}^{3+}$  ions takes place.

**3.1.1. XRD Pattern, Photoluminescence, and PLE Spectra.** The XRD patterns for samples 4, 5, and 6 in Figure 1 indicated

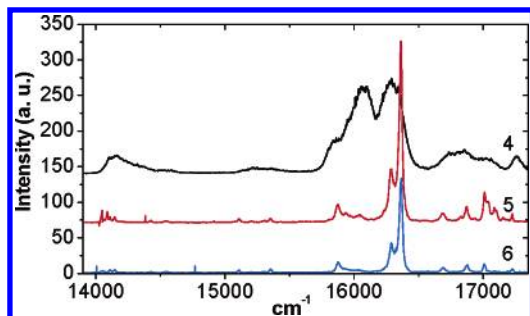


**Figure 5.** 5. Emission spectra of Gd<sub>2</sub>O<sub>3</sub>:Eu<sup>3+</sup> excited by 355 nm at 77 K: a, sample 4 (15 nm); b, sample 5 (23 nm); and c, sample 6 (135 nm).

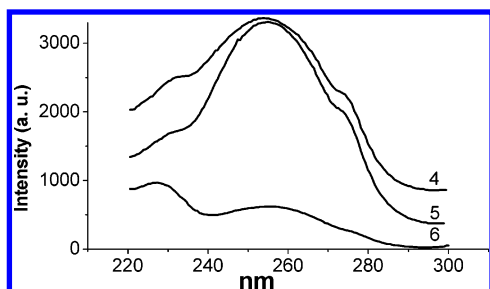


**Figure 6.** 6. The photoluminescence excitation spectra of Gd<sub>2</sub>O<sub>3</sub>:Eu<sup>3+</sup>: a, sample 4; b, sample 5; and c sample 6, monitoring the 611 nm emission.

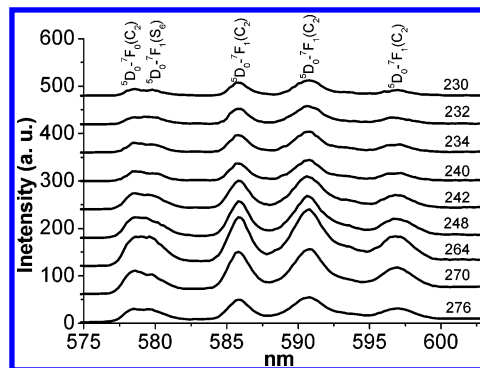
a cubic phase for them all. Samples 4, 5, and 6 annealed at 600, 800, and 1000 °C, respectively, and have different sizes with decreasing line widths. The particle sizes for samples 4, 5, and 6 were determined to be 15, 23, and 135 nm from the XRD results, respectively.

Figure 5 is the photoluminescence spectra for samples 4, 5, and 6 under 355 nm excitation. It is worth noting that these samples show different spectral line widths, while the rare-earth 4f–4f transition spectral lines are supposed to be sharp. The line widths of the PL spectral lines are decreasing with sample number increasing from 4 to 6. The line widths of an electromagnetic transition inside the 4f subshell are widened due to interaction of an electron with the nanocrystalline field. The PL spectra consist of several emission peaks at 578, 592, and 611 nm corresponding to the Eu<sup>3+</sup> 4f–4f <sup>5</sup>D<sub>0</sub> → <sup>7</sup>F<sub>*i*</sub> (*i* = 0, 1, 2) transitions. In the excitation spectrum in Figure 6 for samples 4, 5, and 6, the charge-transfer band (CTB) and the host excitations are found to be at 250 and 230 nm, respectively.<sup>9</sup> In the Eu–O couple the excitation energy of CTB could be estimated by using the following equation by Jorgensen<sup>8</sup>

$$\sigma = [\chi(x) - \chi(M)] \times (3 \times 10^4) \text{ (cm}^{-1}\text{)} \quad (1)$$

Here  $\sigma$  denotes the position of the CTB (in cm<sup>-1</sup>).  $\chi(x)$  and  $\chi(M)$  are the optical electronegativity of the anion and the central metal ion, respectively. For  $\chi(\text{O}) = 3.2$  and  $\chi(\text{Eu}) = 1.75$ , the Eu–O CTB position should be 42 000 cm<sup>-1</sup>, about 238 nm. The CTB position from the PLE spectrum is at 250 nm.

The <sup>8</sup>S<sub>7/2</sub>–<sup>6</sup>I<sub>9/2</sub> transition of Gd<sup>3+</sup> at 276 nm was also observed in the PLE spectrum in Figure 6. The excitation spectral envelope can be decomposed into the host and CTB excitation contribution. The ratios (*A*<sub>1</sub>/*A*<sub>2</sub>) of the integrated intensities of both bands (*A*<sub>1</sub> and *A*<sub>2</sub>) are 1.05, 0.57, and 0.65 for sample 4 (135 nm), sample 5 (23 nm), and sample 6 (15 nm), respectively. The excitations from both bands for the Eu<sup>3+</sup> <sup>5</sup>D<sub>0</sub> → <sup>7</sup>F<sub>2</sub> transition are found to be almost equality in sample 4. With decreasing the size the excitations from the host band



**Figure 7.** 7. Emission spectra excited by the different wavelengths from CTB.

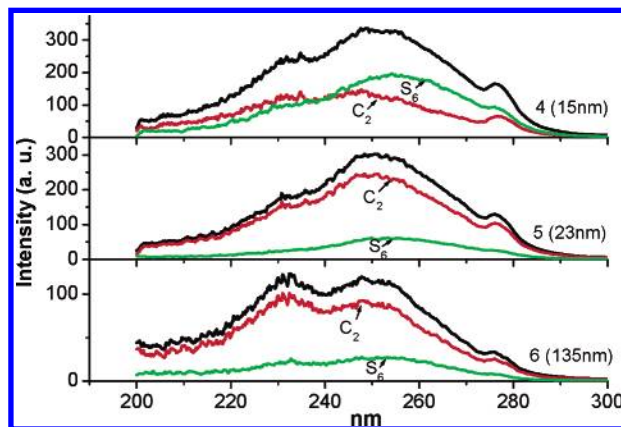


**Figure 8.** 8. Photoluminescence excitation spectra: the topside curve monitoring 578 and 580 nm peaks simultaneously; the C<sub>2</sub> curve monitoring the 578 nm peak; the S<sub>6</sub> curve monitoring the 580 nm peak.

get smaller than that from CTB for both samples 5 and 6, monitoring the Eu<sup>3+</sup> <sup>5</sup>D<sub>0</sub> → <sup>7</sup>F<sub>2</sub> transition peaking at 611 nm.

**3.1.2. The CTB Excitations of Two Sites of Eu<sup>3+</sup> in nano-Gd<sub>2</sub>O<sub>3</sub>:Eu<sup>3+</sup>.** Cubic Gd<sub>2</sub>O<sub>3</sub>:Eu<sup>3+</sup> is known as the c-type oxide lanthanide showing the Ia3 (Th<sup>7</sup>) space point groups.<sup>7</sup> There are two crystallographic sites in lanthanides which are identified as C<sub>2</sub> and S<sub>6</sub> sites. The two kinds of sites are randomly distributed in two different crystallographic sites in Ln<sub>2</sub>O<sub>3</sub> except for gadolinium oxide. The magnetic and electronic transitions are partially allowed on the C<sub>2</sub> sites. In nanocrystallines the Judd–Ofelt theory can be used to determine the radiative transition intensity. The luminescence intensity on the C<sub>2</sub> is higher than that of the S<sub>6</sub> site in the cubic Gd<sub>2</sub>O<sub>3</sub>:Eu<sup>3+</sup> nanocrystallines.

It is shown in Figure 7 the <sup>5</sup>D<sub>0</sub> → <sup>7</sup>F<sub>0</sub> transition at 578 nm from the C<sub>2</sub> and the <sup>5</sup>D<sub>0</sub> → <sup>7</sup>F<sub>1</sub> from the S<sub>6</sub> at 580 nm for sample 5 (emission spectra of samples 4 and 6 are similar) excited by a series of energy excitations from the CTB range. The excitation spectra versus different monitoring positions for samples 4–6 are shown in Figure 8 where the C<sub>2</sub> and S<sub>6</sub> curves are associated with the monitoring wavelength of 578 and 580 nm, respectively, and the top curve corresponds to 578 and 580 nm monitored simultaneously. With decreasing sizes of nanoparticle Gd<sub>2</sub>O<sub>3</sub>:Eu<sup>3+</sup>, the excitations from the S<sub>6</sub> sites are found to be getting much stronger and finally exceed that from the C<sub>2</sub> sites. As we have known, the S<sub>6</sub> site features higher symmetry and energy than the C<sub>2</sub> site. It is concluded that the variation of excitation wavelengths from the C<sub>2</sub> and S<sub>6</sub> sites may be due to the changes of symmetry and energy for the nanosized samples 5 and 6.

**3.2. Calculated J–O Parameters and Quantum Efficiency of the <sup>5</sup>D<sub>0</sub> Level.** **3.2.1. Experimentally Determined Judd–**

*Ofelt Parameters.* According to the Juddy–Ofelt theory, the transitions between the initial and final states in europium crystals belong to the uniform electronic configuration  $4f^6$  and they are parity forbidden. For the transitions between  $J$  and  $J'$  energy levels, the following conditions are assumed in order to simplify the calculation: (1)  $4f^n$  coordinate energy levels are regarded as the linear combination of the Russell–Saunders correlated levels (interspaced states); (2) the particles are equally populated on the sublevels of the initial  $J$  levels; (3) the energy levels of the particles in the  $4f^n$  configuration are higher than the original energy state level  $J$ ; and (4) simplified local field. Finally, Einstein's coefficient of spontaneous emission is quoted as<sup>3</sup>

$$A_{0-\lambda} = \frac{4e^2\omega^3}{3\hbar c^3} \chi \sum_{\lambda=2,4} \Omega_{\lambda} \langle {}^5D_0 || U^{\lambda} || {}^7F_{\lambda} \rangle^2 \quad (2)$$

where  $\chi = n_{\lambda}(n_{\lambda}^2 + 2)/9$  is the Lorentz local field correction, in which  $n_{\lambda}$  is determined from the single term Sellmeier equation<sup>10</sup>

$$\frac{1}{n_{\lambda}^2 - 1} = \frac{-A}{\lambda^2} + B \quad (3)$$

where  $A = 62 \times 10^{-16} \text{ m}^2$  and  $B = 0.3163$ .  $\Omega_{\lambda}$  ( $\lambda = 2, 4$ , and 6) denotes the spectral intensity parameter, determined by the coordinate characteristics of the host material. The transition matrix elements have been examined in ref 11.  $A_{0-\lambda}$  could also be obtained from the relationship

$$A_{0-\lambda} = A_{0-1} \frac{S_{0-\lambda} \sigma_{\lambda}}{S_{0-1} \sigma_1} \quad (4)$$

$S_{0-\lambda}$  is the area under the spectral line of the  ${}^5D_0 \rightarrow {}^7F_{\lambda}$  transition in Figure 5.  $\sigma_{\lambda}$  is the energy barycenter of  $0\text{--}EnDashEnDash\lambda$  transition and  $A_{0-1}$  is Einstein's coefficient of magnetic dipole transition of  ${}^5D_0 \rightarrow {}^7F_1$ .  $S_{0-\lambda}$  and  $\sigma_{\lambda}$  can be measured in the fluorescent spectra of europium. From (2) and (4) we can calculate the intensity parameters  $\Omega_{\lambda}$ .

Next, we calculate  $A_{0-1}$ . The magnetic dipole operator is  $\mathbf{M} = (e/2m)\sum_i(l_i + 2s_i) = (e/2m)(L + 2S)$ . The magnetic dipole matrix element for the states of the same parity is expressed as<sup>2,3</sup>

$$\langle f^n \Psi J J_z | (L + 2S)_q | f^n \Psi' J' J'_z \rangle = (-1)^{J-J_z} \begin{pmatrix} J & 1 & J' \\ -J_z & q & J'_z \end{pmatrix} \times ([f^n \Psi] J || L + 2S || [f^n \Psi'] J') \quad (5)$$

The matrix elements  $\langle {}^5D_0 || L + 2S || {}^7F_1 \rangle$  calculated by using these wave functions in intermediate coupling are given as<sup>12</sup>

$$\begin{aligned} |{}^5D_0\rangle &= -0.2381|{}^7F\rangle - 0.1969|{}^5D\rangle + 0.6893|{}^5D'\rangle - 0.5390|{}^5D''\rangle \\ |{}^7F_1\rangle &= 0.9742|{}^7F\rangle - 0.0027|{}^5P\rangle + 0.0052|{}^5D\rangle + 0.1472|{}^5D'\rangle \\ &\quad - 0.1645|{}^5D''\rangle + 0.0263|{}^5F\rangle + 0.0162|{}^5F'\rangle \end{aligned} \quad (6)$$

Then  $A_{0-1}$  can be written as

$$A_{0-1} = 10^{42} \nu^3 n^3 \frac{(L + 2S)^2}{g_J} \quad (7)$$

**TABLE 1: Some Data of nano-Gd<sub>2</sub>O<sub>3</sub>:Eu<sup>3+</sup> and Bulk Y<sub>2</sub>O<sub>3</sub>:Eu<sup>3+</sup>**

		$\Omega_2,$ $10^{-20} \text{ cm}^2$	$\Omega_4,$ $10^{-20} \text{ cm}^2$	$\tau, \text{ ms}$	$\eta, \%$	refs
Gd <sub>2</sub> O <sub>3</sub> :Eu <sup>3+</sup>	4 (15 nm)	5.61	1.57	1.43	4.6	this work
	5 (23 nm)	3.50	1.08	2.04	5.4	this work
	6 (135 nm)	5.28	1.66	1.41	23.6	this work
Y <sub>2</sub> O <sub>3</sub> :Eu <sup>3+</sup>	bulk	6.31	0.66		15	

where  $g_J$  is the statistical weight ( $2J + 1$ ) of the excited state<sup>13</sup> and  $\nu$  is the transition frequency. The results calculated following the above-mentioned procedure are given in Table 1. The various values of  $\Omega_2$  and  $\Omega_4$  correspond to the variation of crystal field environment, resulting from the different sizes of nano-Gd<sub>2</sub>O<sub>3</sub>:Eu<sup>3+</sup>. To our knowledge, there is no report on the calculation of the J–O parameter of bulk Gd<sub>2</sub>O<sub>3</sub>:Eu<sup>3+</sup>. Gd<sub>2</sub>O<sub>3</sub>:Eu<sup>3+</sup> is basically similar to Y<sub>2</sub>O<sub>3</sub>:Eu<sup>3+</sup> in crystal structure, except for the ionic radii of the rare earth ions ( $R_{\text{Gd}^{3+}} = 0.94 \text{ \AA}$ ,  $R_{\text{Y}^{3+}} = 0.90 \text{ \AA}$ ). The  $\Omega_{\lambda}$  ( $\lambda = 2, 4$ ) of Gd<sub>2</sub>O<sub>3</sub>:Eu<sup>3+</sup> nanoparticles is, however, significantly different from that of bulk Y<sub>2</sub>O<sub>3</sub>:Eu<sup>3+</sup> (see Table 1). Such differences are expected due to the confinement effects on the vibrational states of impurity ions in the surface, whose optical properties are modified by the disorder in the surface, and the alteration of the electronic bands of the matrix.<sup>14</sup> By the selection rules of Eu<sup>3+</sup> ions, the transition from  $J = 0 \rightarrow J'$  (even) is electric dipole allowed. The  ${}^5D_0 \rightarrow {}^7F_6$  transition is, however, 850 nm beyond the visible region. The  $\Omega_6$  is not able to be determined experimentally by the visible spectra, but it is estimated to be  $\Omega_6 < 5 \times 10^{-21} \text{ cm}^2$ .<sup>15</sup>

**3.2.2. Lifetime and Quantum Efficiency of the  ${}^5D_0$  Level.** The fluorescence decay constants and corresponding spectral positions for  ${}^5D_0 \rightarrow {}^7F_J$  ( $J = 0, 1, 2, 3, 4$ ) transitions are listed in Table 2. For the every fixed emission of  ${}^5D_0 \rightarrow {}^7F_J$  ( $J = 0, 1, 2, 3, 4$ ), the decay time is shortened gradually by decreasing the diameters of Gd<sub>2</sub>O<sub>3</sub>:Eu<sup>3+</sup> nanoparticles. In nanocrystalline the shortened lifetime was reported by 5 orders of magnitude, and quantum efficiency increased by about 18% compared with that of bulk.<sup>16</sup> Our results are consistent with the published data, except that the lifetime does not show a drastic drop in the 5 orders of magnitude.

The luminescence quantum efficiency  $\eta$  is defined as the ratio between the number of photons emitted by the Eu<sup>3+</sup> ion and the number of photons absorbed by the Eu<sup>3+</sup> ion. Quantum efficiency is a balance between radiative and nonradiative processes in the sample. The lifetime  $\tau$ , nonradiative  $A_{\text{NR}}$ , and radiative  $A_{\text{R}}$  rates are related by the following equation

$$A_{\text{T}} = \frac{1}{\tau} = A_{\text{R}} + A_{\text{NR}} \quad (8)$$

where the  $A_{\text{R}}$  denoting the sum over the radiative rates  $A_{0-J}$  for each  ${}^5D_0 \rightarrow {}^7F_J$  transition is given by

$$A_{\text{R}} = \sum_J A_{0-J} \quad (9)$$

The emission quantum efficiency of the radiative  ${}^5D_0$  level is given by

$$\eta = \frac{A_{\text{R}}}{A_{\text{R}} + A_{\text{NR}}} \quad (10)$$

The emission quantum efficiency for three samples (Table 1) obtained from eq 10 is 4.6%, 5.4%, and 23.6%, respectively. The charge transfer state (CTS) favors nonradiation de-excitation

TABLE 2: Decay Time and Corresponding Spectral Line Positions of nano-Gd<sub>2</sub>O<sub>3</sub>:Eu<sup>3+</sup>

$L'S'J'$	4 (15 nm)		5 (23 nm)		6 (135 nm)	
	cm <sup>-1</sup>	ms	cm <sup>-1</sup>	ms	cm <sup>-1</sup>	ms
<sup>7</sup> F <sub>0</sub>	17260	0.221 ± 0.002	17221	0.201 ± 0.001	17221	1.403 ± 0.011
<sup>7</sup> F <sub>1</sub>	16830	0.235 ± 0.002	17002	0.208 ± 0.001	17016	0.932 ± 0.004
<sup>7</sup> F <sub>2</sub>	16314	0.258 ± 0.002	16373	0.966 ± 0.004	16373	1.048 ± 0.005
<sup>7</sup> F <sub>3</sub>	15366	0.228 ± 0.002	15881	0.967 ± 0.004	15881	1.020 ± 0.005
<sup>7</sup> F <sub>4</sub>	14172	0.210 ± 0.002	14061	0.935 ± 0.005	14129	1.064 ± 0.007

of the <sup>5</sup>D<sub>0</sub> level toward the <sup>7</sup>F multiplet, with an activation energy of  $\Delta E_i$ ,

$$A'_{\text{NR}} = A_{\text{CTS}} \exp(-\Delta E_i/kT) \quad (11)$$

where  $A_{\text{CTS}}$  is the de-excitation rate of the CTS toward <sup>7</sup>F levels. The host lattice vibrations create the changes in the electric field around an ion, resulting in the multiphonon nonradiation de-excitation. The de-excitation rate can be described by semiempirical law as:

$$A_{\text{NRmp}} = A_{\text{mp}}(0)[1 + \bar{n}_i]^{p_i} \quad (12)$$

$A_{\text{mp}}(0)$  is the rate constant at 0 K,  $p_i$  the number of phonon involved, and  $\bar{n}_i$  the Bose thermal occupation number of the  $i$ th phonon mode. On the other hand, cross relaxation like  $\text{Eu}^{3+}({}^5\text{D}_1) + \text{Eu}^{3+}({}^7\text{F}_0) \rightarrow \text{Eu}^{3+}({}^5\text{D}_0) + \text{Eu}^{3+}({}^7\text{F}_3)$  will occur at higher Eu<sup>3+</sup> doping concentration (>3%). The cross relaxation plays an important role in the radiative and nonradiative processes.

#### 4. Conclusions

The Eu<sup>3+</sup> doped monoclinic and cubic Gd<sub>2</sub>O<sub>3</sub> nanocrystallines are shown with different PL and PLE spectral properties. The site -selective excitation spectrum was used as a powerful means to identify structural sites. The crystal field environment in impurity-doped nanocrystallines posed an important impact on the luminescence decay time. A new point of view to study the spectroscopic properties of Gd<sub>2</sub>O<sub>3</sub>: Eu<sup>3+</sup> nanocrystallines could be proposed under the excitations of CTB. The integral intensities of the excitation spectra of  $\text{Eu}^{3+} {}^5\text{D}_0 \rightarrow {}^7\text{F}_2$  for the

bulk are equal under the excitations from the host and CTB, but obviously different for the Gd<sub>2</sub>O<sub>3</sub>:Eu<sup>3+</sup> nanocrystallines with distinct sizes. The spectral intensity parameters  $\Omega_\lambda$  were calculated by using the J–O theory for bulk and nanoscale materials with different sizes. The spectral intensity parameters varied with the crystal field environment in nanoscale materials.

**Acknowledgment.** The support of the Natural Science Foundation of China under project grant Nos. 60308008 and 10274083 is gratefully acknowledged. The authors would like to thank Profs. Shaozhe Lu and Xinguang Ren for their assistance in the spectral experiments.

#### References and Notes

- (1) Dexpert-Ghys, J.; Faucher, M.; Caro, P. *Phys. Rev. B* **1981**, *23*, 607.
- (2) Judd, B. R. *Phys. Rev.* **1962**, *127*, 750.
- (3) Ofelt, G. S. *J. Chem. Phys.* **1962**, *37*, 511.
- (4) de Sa, G. F.; Malta, O. L.; de Mello Donega, C.; Simas, A. M.; Longo, R. A.; Santa-Cruz, P. L.; da Silva, E. F., Jr. *J. Mol. Struct. Coord. Chem. Rev.* **2000**, *196*, 165.
- (5) Tao, Y.; Zhang, G.; Xia, S. *Mater. Res. Bull.* **1997**, *32*, 501.
- (6) Hoefdraad, H. E. *J. Solid State Chem.* **1975**, *15*, 175.
- (7) Buijs, M.; Meyerink, A.; Blass, G. *J. Lumin.* **1987**, *37*, 9.
- (8) Jorgensen, C. K. *Prog. Inorg. Chem.* **1970**, *12*, 101.
- (9) *Opt. Mater.* **2003**, *23*, 547.
- (10) Medenbach, O.; Dettmar, D.; Shannon, R. D.; Fischer, R. X.; Yen, W. M. *J. Opt. A: Pure Appl. Opt.* **2001**, *3*, 174.
- (11) Carna, W. T.; Crosswhite H.; Crosswhite, H. M. Argonne National Laboratory Report, unnumbered, 1977.
- (12) Ofelt, G. S. *J. Chem. Phys.* **1963**, *38*, 2171.
- (13) Detrio, J. A. *Phys. Rev. B* **1971**, *4*, 1422.
- (14) Meitzer, R. S.; Feofilov, B. S.; Tissue, P.; Yuan, H. B. *Phys. Rev.* **1999**, *20*, R14012.
- (15) Krupke, W. F. *Phys. Rev.* **1966**, *145*, 325.
- (16) Bhargava, R.; Gallagher, D.; Hong X.; Nurmikko, A. *Phys. Rev. Lett.* **1994**, *72*, 416.